Journal of Fluids and Structures 18 (2003) 455–465

JOURNAL OF FLUIDS AND STRUCTURES

www.elsevier.nl/locate/jnlabr/yjfls

Numerical solutions of a viscous uniform approach flow past square and diamond cylinders

C. Dalton[a,*], W. Zheng[b]

[a] *Department of Mechanical Engineering, University of Houston, Houston, TX 77204-4006, USA*
[b] *Consultant, Houston, TX, USA*

Received 28 November 2002; accepted 11 July 2003

Abstract

Numerical results are presented for a uniform approach flow past square and diamond cylinders, with and without rounded corners, at Reynolds numbers of 250 and 1000. This unsteady viscous flow problem is formulated by the 2-D Navier–Stokes equations in vorticity and stream-function form on body-fitted coordinates and solved by a finite-difference method. Second-order Adams-Bashforth and central-difference schemes are used to discretize the vorticity transport equation while a third-order upwinding scheme is incorporated to represent the nonlinear convective terms. A grid generation technique is applied to provide an efficient mesh system for the flow. The elliptic partial differential equation for stream-function and vorticity in the transformed plane is solved by the multigrid iteration method. The Strouhal number and the average in-line force coefficients agree very well with the experimental and previous numerical values. The vortex structures and the evolution of vortex shedding are illustrated by vorticity contours. Rounding the corners of the square and diamond cylinders produced a noticeable decrease on the calculated drag and lift coefficients.

1. Introduction

A uniform approach flow past a bluff cylinder generates a periodic, alternating shedding of vortices from the body above a minimum value of Reynolds number ($\mathrm{Re} = Ud/v$). The Strouhal number ($\mathrm{St} = fd/U$) characterizes the frequency of vortex shedding. In these two definitions, f is the shedding frequency, d is the cylinder diameter or side, v is the kinematic viscosity, and U is the uniform approach velocity. Our main objective in this numerical study is to obtain drag and lift coefficients and examine the effects of rounding the corners on square and diamond cylinders on these coefficients. The application of this square-cylinder study will be primarily toward the design of offshore structures. Even though our Reynolds numbers, up to 1000, are much smaller than the values expected in practice, insight will be gained on the effects of rounding the corners.

There are some experimental and numerical studies of the vortex-shedding flow past rectangular cylinders: however, few quantitative experimental studies can be found which include in-line force and lift coefficients. Delaney and Sorensen (1953) performed one of the earliest experimental studies on square and diamond cylinders, as well as other cylindrical shapes. However, this study concentrated on determination of drag coefficients and did not report any lift coefficient data and, to use their own terminology, meager Strouhal number data. Since the Delaney and Sorensen study was at Re values much higher than those for which any accurate computational studies are available, we will not include further reference to this study in spite of its relevance to the overall subject.

*Corresponding author.
E-mail address: dalton@uh.edu (C. Dalton).

0889-9746/$ - see front matter
doi:10.1016/j.jfluidstructs.2003.07.010

Relevant computational studies at similar values of Re for flow past a square cylinder have been reported by Davis and Moore (1982). Franke et al. (1990), Kim and Benson (1992), Okajima et al. (1992), Saha et al. (2000), and Sohankar et al. (1995, 1997, 1998). Experimental studies for similar values of Re have been by Davis and Moore (1982), Okajima (1982), and Norberg (1993). The only study found for a diamond-shaped cylinder (or a square cylinder with the flow at a 45° angle of attack) is by Torii et al. (2000). The effort by Torii et al. covered both experimental and numerical descriptions of the problems. All of the above studies were for square-cornered cylinders. The only study found that dealt with rounded corners was by Tamura et al. (1990). However, this study was for a square cylinder at $\mathrm{Re} = 10^5$, but which included no turbulence modelling, even at this large a value of Re.

There have been many studies, both numerical and experimental, that have considered flow past square cylinders at higher values of Re. Various forms of turbulence modelling have been included in most of the higher Re studies. However, our emphasis here is the contrast between square and rounded corners for both square- and diamond-shaped cylinders. Thus, our review does not include any higher Re cases, but was restricted to those cases that can be and have been modelled as viscous flow solutions. This study is a continuation of our earlier effort on oscillating flow past cylinders with sharp corners (see Zheng and Dalton, 1999).

With the aid of powerful computational facilities and advanced numerical techniques, including the grid generation technique and the multigrid method, the present study provides a general and robust approach to investigate viscous flow past bluff bodies, which is concentrated on square cylinders. This numerical study will be concerned with uniform approach flow for a viscous fluid. The pattern of vortex shedding and the variation of the force coefficients as well as the Strouhal number will be investigated.

2. Mathematical formulation

The uniform approach flow of a viscous incompressible fluid past a square cylinder is considered. The governing equations for a 2-D unsteady flow are the Navier–Stokes equations in the vorticity and stream-function form, which can be expressed nondimensionally in Cartesian coordinates as

$$\omega_t + \psi_y \omega_x - \psi_x \omega_y = \frac{1}{\mathrm{Re}}(\omega_{xx} + \omega_{yy}), \tag{1}$$

$$\psi_{xx} + \psi_{yy} = -\omega, \tag{2}$$

where the Reynolds number, Re, was defined earlier, ψ is the 2-D stream function, and ω is the z-direction vorticity. For the uniform approach flow past the cylinder, the boundary conditions are

$$\psi = \frac{\partial \psi}{\partial n} = 0, \quad \omega = \omega_b \quad \text{on the cylinder}, \tag{3}$$

$$\psi = \psi_p, \quad \omega = 0 \quad \text{far from the cylinder}, \tag{4}$$

where n is the unit normal to the surface of the cylinder. The vorticity distribution on the surface of the cylinder is ω_b and is determined by imposing the no-penetration and no-slip boundary conditions on the Poisson equation, Eq. (2). The starting solution for the stream function for potential flow past the rectangular cylinders is ψ_p and is obtained through the Schwartz-Christoffel transformation.

For a bluff body in a doubly connected region R bounded by an arbitrary contour Γ, a branch cut in the physical plane is introduced to generate a simply connected rectangular computational domain. A one-to-one transformation from the physical plane (x, y) to a generalized curvilinear coordinate plane (ξ, η) is established to make the segments of the boundary contour in the physical plane coincide with particular curvilinear coordinate lines in the transformed plane, which is defined by

$$x = x(\xi, \eta), \quad y = y(\xi, \eta). \tag{5}$$

Under the coordinate transformation, the governing Eqs. (1) and (2) can be mapped into the corresponding equations containing partial derivatives with respect to ξ and η as follows:

$$\frac{1}{\mathrm{KC}}\omega_t + \frac{1}{J}(\psi_\eta \omega_\xi - \psi_\xi \omega_\eta) = \frac{1}{\mathrm{Re}}\bar{\Delta}\omega, \tag{6}$$

$$\bar{\Delta}\psi = -\omega, \tag{7}$$

where the operator $\bar{\Delta}$ is defined by

$$\bar{\Delta}A = \frac{\alpha A_{\xi\xi} - 2\beta A_{\xi\eta} + \gamma A_{\eta\eta}}{J^2} + (1/J^3) \times [(\alpha x_{\xi\xi} - 2\beta x_{\xi\eta} + \gamma x_{\eta\eta})(y_\xi A_\eta - y_\eta A_\xi) + (\alpha y_{\xi\xi} - 2\beta y_{\xi\eta} + \gamma y_{\eta\eta})(x_\eta A_\xi - x_\xi A_\eta)] \tag{8}$$

with A as either ψ or ω. The transformation parameters are

$$J = x_\xi y_\eta - x_\eta y, \quad \alpha = x_\eta^2 = y_\eta^2, \quad \beta = x_\xi x_\eta + y_\eta y_\xi, \quad \gamma = x_\xi^2 y_\xi^2. \tag{9}$$

The boundary conditions under the transformation become

$$\psi = \frac{\gamma^{(1/2)}\psi_\eta}{J} = 0, \quad \omega = \frac{\gamma\psi_{\eta\eta}}{J^2}, \quad \text{both on } \eta = 0 \tag{10}$$

and for a uniform approach flow,

$$\psi = \psi_p, \quad \omega = 0 \quad \text{both on } \eta = 1. \tag{11}$$

The periodic boundary conditions are imposed on $\xi = 0$ and $\xi = 1$. The initial conditions are

$$\psi = \psi_p, \quad \text{in the flow field for a uniform approach flow.} \tag{12}$$

The pressure coefficient is derived from the integration of the momentum equation along the surface of the cylinder, which is given in the transformed plane by

$$C_p = \frac{1}{\mathrm{Re}} \int_0^\xi \frac{1}{J}(\beta\omega_\xi - \gamma\omega_n)\mathrm{d}\xi. \tag{13}$$

The in-line force and lift coefficients in the transformed plane are denoted by C_F and C_L, respectively, and are given by

$$C_F = 2\int_0^1 \left(y_\xi C_P - \frac{1}{\mathrm{Re}} x_\xi \omega\right) \mathrm{d}\xi, \tag{14}$$

$$C_L = -2\int_0^1 \left(x_\xi C_P + \frac{1}{\mathrm{Re}} y_\xi \omega\right) \mathrm{d}\xi. \tag{15}$$

3. Numerical implementation

In the present computation, the grid systems are produced by GENIE2D, a grid-generation package created at the NSF Engineering Research Center at Mississippi State University, using the algebraic grid generation method [see Thames et al. (1977)]. The grid system for a square cylinder with rounded corners is shown in Fig. 1. Apart from the grid concentration very close to the body surface in the radial direction, grid concentration is also arranged locally near the four sharp corners of the square cylinder to increase numerical resolution near the corners with very large gradients of velocity and vorticity. All of the transformation derivatives and parameters in Eq. (9) are approximated by second-order central-difference expressions.

The vorticity transport equation is explicitly discretized in time by using the second-order Adams-Bashforth scheme. All of the spatial discretizations are second-order central-difference schemes except the convective terms. The third-order upwinding scheme proposed by Leonard (1979) is applied to approximate these convective terms. Due to the existence of mixed derivatives and variable coefficients in the elliptic partial differential Eq. (7), it is impractical to solve this equation by using the spectral method incorporating the FFT algorithm with high efficiency. The multigrid iteration method is a very efficient approach to solve Eq. (7).

A multigrid solver, developed by Sanders (1992) for the 2-D Helmholtz equation, was used for this solution; it is of the form

$$(a(x)\nabla u) - \alpha u + g(x) = 0, \tag{16}$$

where $a(x), f(x)$ and $u(x, y)$ are arbitrary functions and α is a constant. In the present study, the multigrid solver has been developed to solve a 2-D elliptic partial differential equation with mixed derivatives, first-order derivatives and the variable coefficients,

$$a_1 u_{xx} + a_2 u_{xy} + a_3 u_{yy} + a_4 u_x + a_5 u_y + a_6 u + g = 0, \tag{17}$$

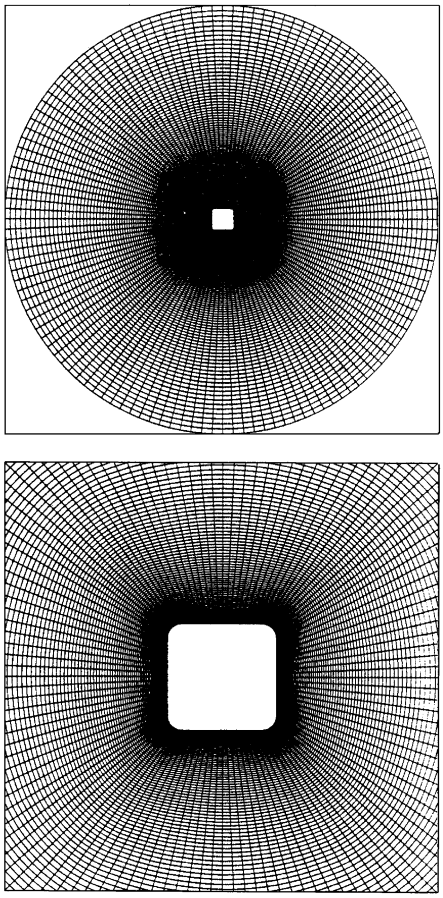

Fig. 1. Grid system for a cylinder with rounded corners.

where $a_1, a_2, a_3, a_4, a_5, a_6, g$, and u are arbitrary functions of x and y. For viscous flow past rectangular cylinders, the grid system is characterized by discontinuous transformation derivatives near the four sharp corners, which correspondingly lead to the strongly discontinuous coefficients in Eq. (9). This multigrid solver has the capability of solving elliptic partial differential equations with discontinuous coefficients. It has been shown in various numerical tests (see Zheng and Dalton, 1999) that this same multigrid solver has a solid dependability of accurately solving elliptic partial differential equations with higher efficiency than SOR iteration method with Chebyshev acceleration. The multigrid solver has been optimized herein at more than 350 megaflops on the Cray C90 at the (now defunct) Pittsburgh Supercomputing Center.

The vorticity boundary condition in Eq. (10) on the body surface can be expressed in terms of the stream function in the interior mesh points with second-order accuracy using the Taylor series expansion with the implication of the no-slip condition,

$$\omega_{i,1} = \frac{\gamma_{i,1}}{(J_{i,1}\Delta\eta)^2}(7\psi_{i,1} - 8\psi_{i,2} + \psi_{i,3})/2, \tag{18}$$

where $\Delta\eta$ is the grid spacing in the η direction in the transformed plane.

4. Results and discussion

A detailed discussion of convergence is presented in Zheng and Dalton (1999) where the analysis is for an oscillating flow rather than a uniform approach flow. The largest Reynolds number, based on the maximum oscillatory velocity, was about 2350 in the Zheng and Dalton study. Three grid sizes were tested (65×65, 129×129, and 257×257) and two types of grids were examined for the circumferential direction (uniform and a hyperbolic tangential distribution with

local grid concentration near the corners). The local grid concentration caused a near corner decrease of the uniform grid size by a factor of four. The calculations for the 257×257 grid were done on the Cray C90 at the Pittsburgh Supercomputing Center and the NEC SX4 at the NEC location in The Woodlands, TX while the others where done in double precision on an SGI Indigo R4000 at the University of Houston. Comparison between experimental and calculated values of drag coefficient revealed that use of the 129×129 grid with local grid concentration, was sufficient to get an accurate solution. This observation has also been justified in Zheng and Dalton (1999). Results from the three different grids, with and without local grid concentration, are shown in the Zheng and Dalton study. These results also revealed that the 129×129 grid was sufficient for convergence. The convergence calculations were not repeated for the uniform flow case.

Another feature of the study is the use of the multigrid solver applied to Eq. (8), which also contains mixed derivatives. Fig. 2 shows a comparison for the 129×129 grid of the L_2 and L_∞ norms for both the multigrid solver and the SOR method with Chebyshev acceleration. It is quite clear that the multigrid method is much more efficient than the SOR method for this problem; convergence is obtained in one-fourth the number of iterations. This is another strong example of the utility of the multigrid method.

Table 1 presents the results for the two values of Reynolds number considered, $\mathrm{Re} = 250$ and 1000, for the square- and rounded-edge square and diamond cylinders. The rounded corners have a radius of $d/8$. Even though tabular results are available for $\mathrm{Re} = 250$, graphical results are presented only for $\mathrm{Re} = 1000$. These results for $\mathrm{Re} = 1000$ are also shown in Figs. 3–6. Figs. 3 and 4 show that the drag coefficient has a higher harmonic for both corner configurations. Fig. 3 shows that the lift coefficient is responding at the vortex shedding frequency for the square corner case and includes (see Fig. 4) higher harmonic behavior when the corners are rounded. The opposite effect is noted for the diamond cylinder. Fig. 5 shows the square-cornered result which shows a fairly prominent beating effect in both lift and drag. When the corners are rounded (Fig. 6) the beating effect is diminished, especially so for the lift behavior.

As seen in Table 1, there is a striking decrease in the value of C_D when the corners are rounded. We attribute this decrease in drag coefficient to the increase in wake pressure for each rounded-corner case. The separating shear layers for each rounded-corner case are not deflected as far from the cylinder as for the square-corner cases. This suggests that the shear layer rollup is not as intense as for the square-corner cases which results in the wake pressure being slightly less negative. This wake-pressure explanation is also supported by the very slight increase in Strouhal number for each case. The increase in shedding frequency means that the vortices being shed in the rounded-corner cases are being shed sooner than those for the square-cylinder cases as is shown in Table 1 in the higher Strouhal number values for the rounded-corner results. The implication is that the wake pressures have less time to be influenced by the roll-up of the attached shear layers. The r.m.s. lift coefficient decreases over 50% for the diamond cylinder at both Reynolds numbers when the corners are rounded. The decrease in r.m.s. lift coefficient for the square cylinder case was only about 8% when the corners were rounded. We attribute this larger decrease (due to rounding) for the diamond cylinder to the slight change in the velocity profile at separation. The separation point for the square-cornered diamond cylinder is fixed at the sharp corner. Conversely, the rounded-corner case, even at the slight rounding ($d/8$) considered herein, provides a slight change in pressure gradient prior to separation. The separating shear layer, with rounding, leads to a less intense shear layer rollup. The result is a lessening of the transverse pressure differences during vortex shedding;

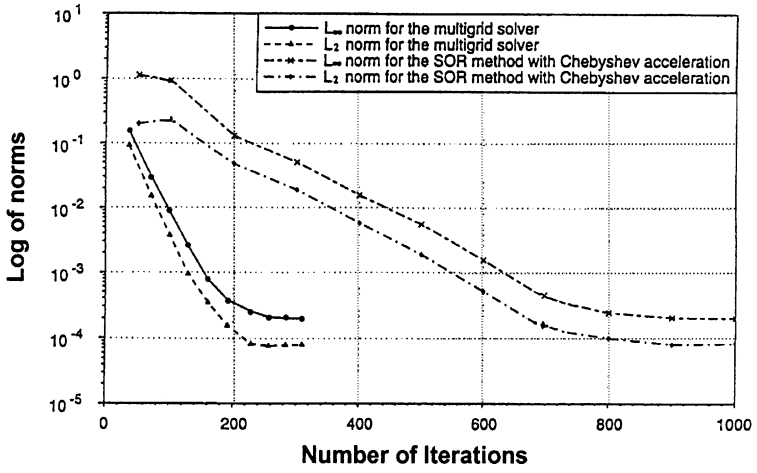

Fig. 2. Comparison of accuracy and efficiency between the multigrid and SOR solvers on a 129×129 grid.

Table 1
Calculated and experimental values

Source	Re	St	C_D	$C_{L,\text{r.m.s.}}$	Type
Present (c)	250	0.16	1.8	0.36	Square, square
Present (c)	250	0.21	2.75	0.56	Diamond, square
Present (c)	250	0.22	1.7	0.22	Diamond, rounded
Present (c)	1000	0.15	2.5	0.85	Square, square
Present (c)	1000	0.16	1.75	0.8	Square, rounded
Present (c)	1000	0.2	2.25	0.8	Diamond, square
Present (c)	1000	0.21	1.65	0.35	Diamond, rounded
Saha et al. (2000) (c)	250	0.142	1.77		Square, square
Davis and Moore (1982) (c)	250	0.165	1.77		Square, square
Franke et al. (1990) (c)	250	0.141	1.67	0.81	Square, square
Okajima (1982) (e)	250	0.141			Square, square
Okajima et al. (1992) (e)	500	0.13	2.1	~1.13	Square, square
Norberg (1993) (e)	300	0.14			Square, square
Norberg (1993) (e)	1000	0.13			Square, square
Sohankar et al. (1995) (e)	200	0.149	1.45	0.36	Square, square
Sohankar et al. (1997) (c)	400	0.13			Square, square
Sohankar et al. (1998) (c)	500	0.126	1.87	1.13	Square, square
Torii et al. (2000) (c)	250	0.11			Diamond, square
Schlichting (1985) (e)	250	0.19			Diamond, square

Note: In the first column, (c) means calculated and (e) means experimental. In the last column, the first word is the cylinder shape and the second word describes the corner configuration.

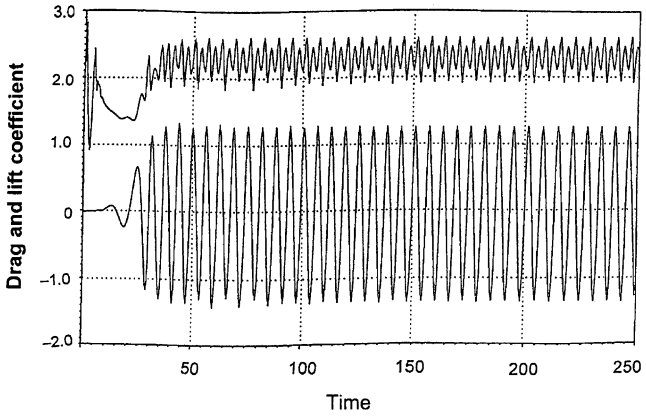

Fig. 3. Force coefficients versus time for a square cylinder with square corners at Re = 1000.

hence, the transverse force decreases for the rounded-corner diamond-cylinder case. The same effect for the square cylinder is much less because the separating shear layer has no streamwise momentum of its own for either the square or rounded-corner cases when separation occurs. This means that the strength of the separating shear layer is virtually unaffected by rounding the corners. The comparison to other results, both experimental and comparison is very good in some cases and poor in others. In fact, there is a noticeable lack of agreement between results of other investigators as well.

4.1. Uniform approach flow past square cylinders

The computation of uniform approach flow past a square cylinder is carried out on a 129×129 grid at Re = 250 and 1000. The grid distribution is uniform in the circumferential direction and exponential in the η direction with the minimum mesh size equal to 0.02 in the transformed plane. Convergence is discussed earlier herein and in Zheng and Dalton (1999). The maximum dimensionless distance between the center of the cylinder and the outer boundary is 25

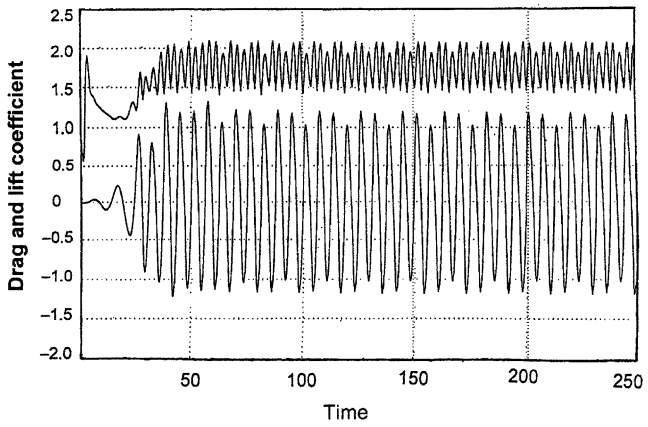

Fig. 4. Force coefficients versus time for a square cylinder with rounded corners at Re = 1000.

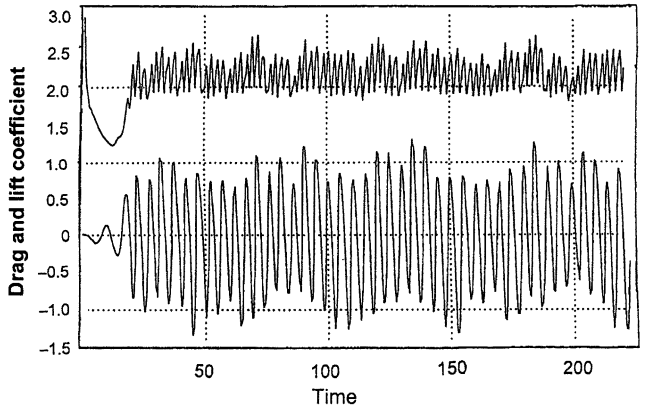

Fig. 5. Force coefficients versus time for a for a diamond cylinder with square corners at Re = 1000.

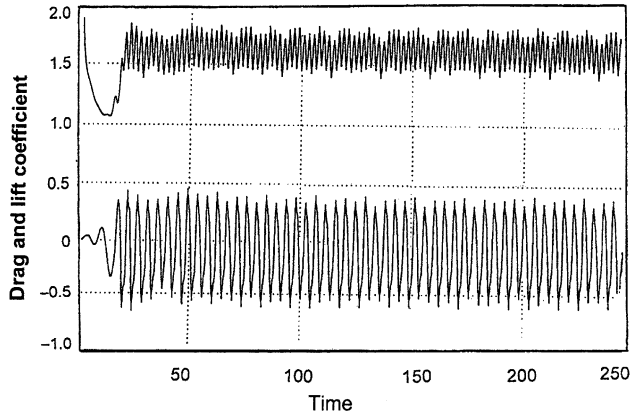

Fig. 6. Force coefficients versus time for a for a diamond cylinder with rounded corners at Re = 1000.

cylinder sides and the side of the square (or diamond) cylinder is specified as 1. The time step Δt is 0.002. The 129×129 grid used in the present study is about four times that in Davis and Moore (1982). To promote an earlier onset of vortex shedding, a small perturbation is imposed on the body surface of the cylinder, i.e., a constant value of $\psi = 0.005$ instead

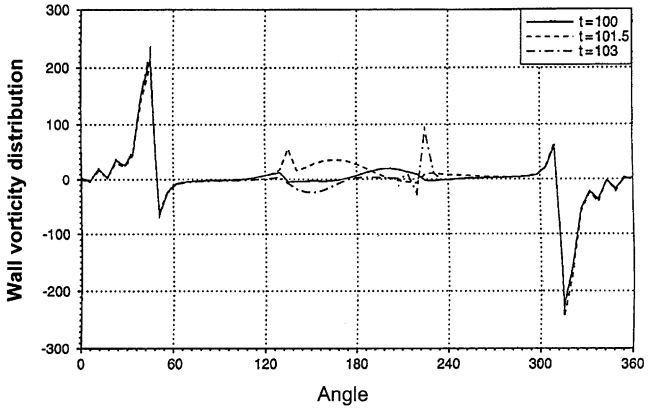

Fig. 7. The wall vorticity versus θ for the square cylinder with square corners at Re = 1000.

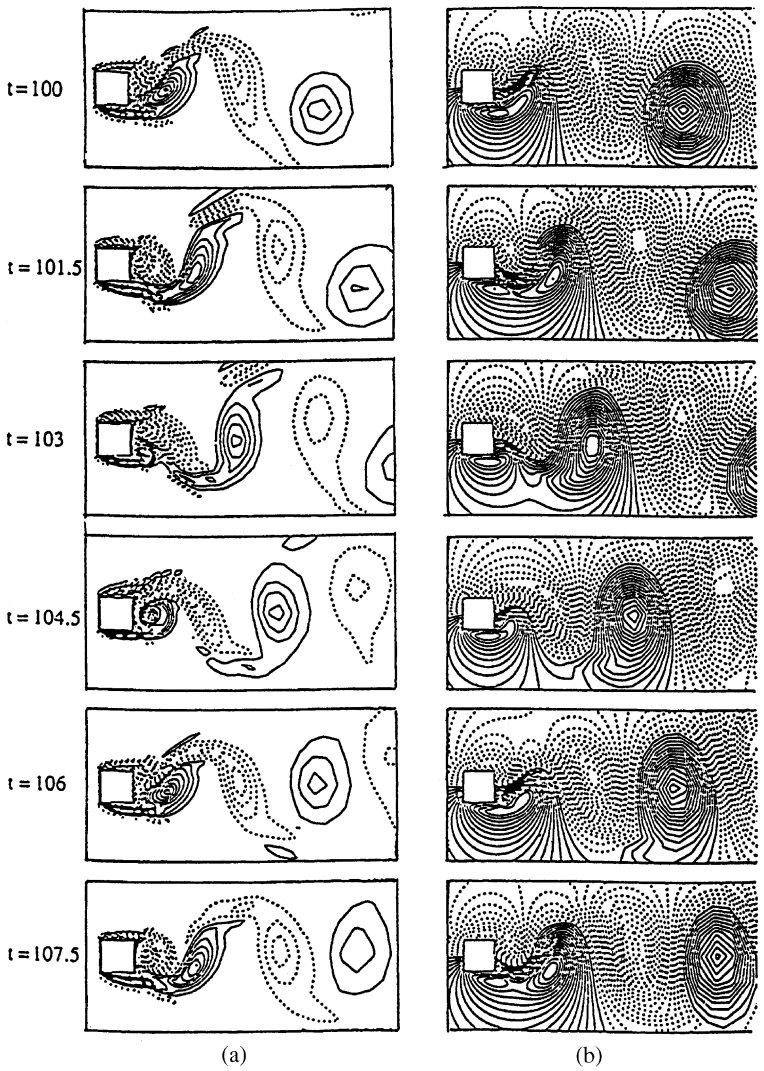

Fig. 8. The near field plots of vorticity contours (a) and streamlines (b) for the square cylinder with rounded corners at Re = 1000.

of zero. The perturbation is removed at time beyond 5, and the inertial effect caused by the small perturbation will vanish as time advances. This same procedure has been used in most of our previous studies and has been found to be very effective.

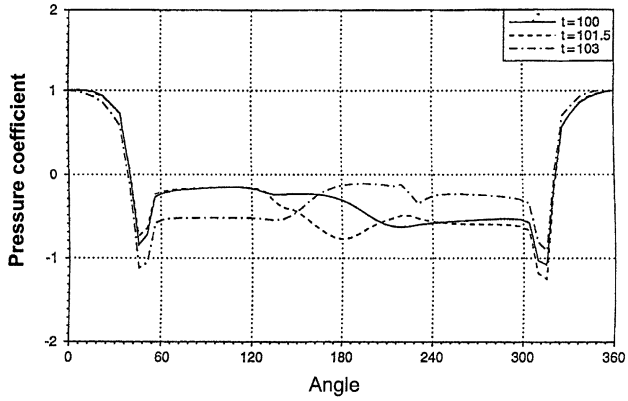

Fig. 9. The pressure coefficient versus θ for the square cylinder with square corners at Re = 1000.

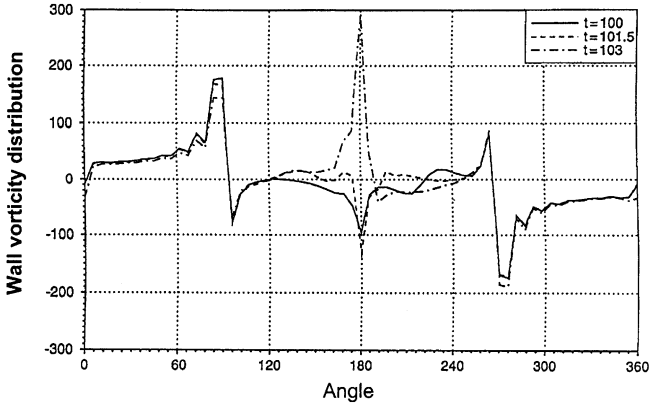

Fig. 10. The wall vorticity versus θ for the diamond cylinder with square corners at Re = 1000.

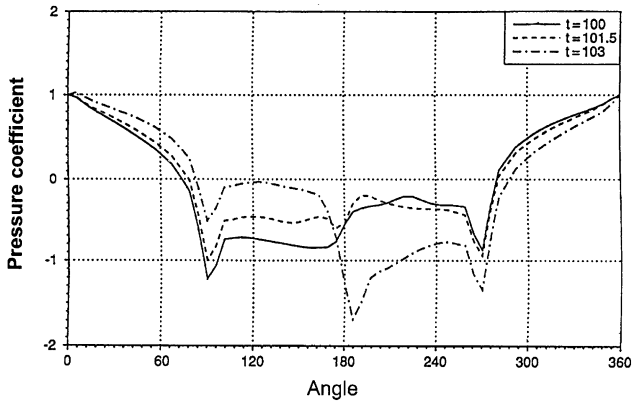

Fig. 11. The pressure coefficient versus θ for the diamond cylinder with square corners at Re = 1000.

Fig. 7 presents the wall-vorticity distribution at Re = 1000 and $t = 100$, 101.5, and 103 for the square-corner cases. The variation of the wall-vorticity distributions has a singular-like distribution at the two front sharp corners of the cylinder. There is a clear indication of separation (due to the sharp change in sign of the wall vorticity) at 45° from the leading edge of the body At 135°, i.e., the rear corners of the cylinder, there again is evidence of separation, but with a time-dependent behavior, in contrast to the upstream corners. The drag and lift coefficients are smooth, periodic and symmetric about the axis of the onset-flow direction at time beyond $t = 100$, as shown in Fig. 3. The appearance of the sub-harmonic in the variation of the drag coefficient at Re = 1000 is similar to the numerical results obtained by Davis and Moore (1982). A near-field view of the wake structure at Re = 1000 is shown in Fig. 8. The Strouhal number is calculated through averaging over a range of vortex-shedding periods which is defined as the time between adjacent peaks in the lift curve, regardless of amplitude variations. It is found that the Strouhal number has little change after averaging more than 20 periods of vortex shedding at time beyond 100. Comparisons of the Strouhal number and the average in-line force coefficient to several experimental and numerical results are shown in Table 1 and are in reasonable agreement. The pressure coefficient plot for this case is shown in Fig. 9 where we see that there is a sharp increase in pressure immediately after separation at the upstream corners. The pressure along the two parallel sides of the cylinder is relatively constant as would be expected, but with a time-dependent influence. This plot is typical of pressure coefficient behavior due to periodic vortex shedding.

4.2. *Uniform approach flow past a diamond cylinder*

Fig. 10 shows the wall vorticity at Re = 1000 and $t = 100$, 101.5, and 103 for the square-cornered diamond cylinder. In this case, separation takes place at 90° on either side of the upstream apex of the cylinder. There is a considerable time-dependent difference in the wall vorticity at the downstream apex.

The diamond cylinder pressure coefficient plot is shown in Fig. 11 where even the pressure values upstream of separation show some time dependence. The wake pressure for the diamond cylinder shows considerably more variation across the wake in both time and position when compared to the square-cylinder result in Fig. 9. This plot shows a sharp change in pressure at separation on each upstream side of the diamond cylinder. This pressure coefficient is also typical for periodic shedding of vortices.

5. Conclusions

Numerical solutions of a viscous uniform approach flow past square and diamond cylinders are obtained from solving the 2-D Navier–Stokes equation in the vorticity/stream-function formation on body-fitted coordinates. A uniform approach flow past a square cylinder is simulated for Re = 250, 1000. At Re = 250, the in-line force and lift coefficients are smooth, periodic and symmetric with respect to the axis of the onset-flow oscillation. At Re = 1000, the appearance of the sub-harmonic in the variation of the in-line force coefficient is similar to the numerical results obtained by Davis and Moore (1982). Comparison of the Strouhal number between the calculated results and the experimental values obtained by Davis and Moore is in reasonable agreement, as are the calculated average in-line force coefficients.

Calculations are done for both square- and rounded-corner cases. Even though the wake at Re = 1000 is clearly turbulent, no turbulence modelling was included. Our purpose was to compare the effects of slight rounding of the corners of the two cylindrical configurations. The results show a considerable effect due to the rounding of the corners, more so for the diamond cylinder than the square cylinder. Even though no turbulence model was incorporated, the upwinding scheme provided a pseudo-LES description. However, we do recognize that turbulence modelling is necessary to gain an accurate solution, even at Re = 1000.

Even though the results presented herein are for a 2-D viscous flow, it is possible to extend this analysis to include a 3-D LES model as is done in Lu et al., 1997 for flow past a circular cylinder. The results strongly indicate that rounding the corners of both square and diamond cylinders has the effect of decreasing the lift and drag for both configurations. The effect on the lift is noticeably greater for the diamond orientation.

Acknowledgements

The authors acknowledge the help of Prof. Richard Sanders in the Department of Mathematics at the University of Houston. We also thank Richard Xu for helping with the last part of the calculations. Support for the second author was provided by the ERAP Program of the Department of Energy through the Texas Higher Education Coordinating

Board. Some of the computer time was provided by the Pittsburgh Supercomputing Center, the San Diego Supercomputing Center, and NEC at The Woodlands, TX.

References

Davis, R., Moore, E.F., 1982. A numerical study of vortex shedding from rectangles. Journal of Fluid Mechanics 116, 475–506.

Delaney, N.K., Sorensen, N.E., 1953. Low speed drag of cylinders of various shapes. NACA TN 3038.

Franke, R., Rodi, W., Schonung, B., 1990. Numerical calculation of laminar vortex shedding for flow past cylinders. Journal of Wind Engineering and Industrial Aerodynamics 35, 237–257.

Kim, S.W., Benson, T.J., 1992. Comparison of the SMAC, PISO and iterative time-advancing schemes for unsteady flows. Computers and Fluids 21, 435–454.

Leonard, B.P., 1979. A stable and accurate convective modeling procedure based on quadratic upstream interpolation. Computer Methods in Applied Mechanics and Engineering 19, 59–98.

Lu, X., Dalton, C., Zhang, J., 1997. Application of large eddy simulation flow past a circular cylinder. Journal of Offshore Mechanics and Arctic Engineering 119, 219–225.

Norberg, C., 1993. Flow around rectangular cylinders: pressure forces and wake frequencies. Journal of Wind Engineering and Industrial Aerodynamics 49, 187–196.

Okajima, A., 1982. Strouhal number of rectangular cylinders. Journal of Fluid Mechanics 123, 379–398.

Okajima, A., Ueno, H., Sakai, H., 1992. Numerical simulation of laminar and turbulent flows around rectangular cylinders. International Journal for Numerical Methods in Fluids 15, 999–1012.

Saha, A.K., Muralidhar, K., Biswas, G., 2000. Transition and chaos in a 2-D flow past a square cylinder. ASCE Journal of Engineering Mechanics 126, 523–532.

Sanders, R., 1992. Personal communication. Department of Mathematics, University of Houston.

Schlichting, H., 1985. Boundary Layer Theory. McGraw-Hill Book Co, New York.

Sohankar, A., Davidson, L., Norberg, C., 1995. Numerical simulation of unsteady flow around a square two-dimensional cylinder. In: Bilger, R.W. (Ed.), Proceedings of the12th Australian Fluid Mechanics Conference. The University of Sydney, Australia, pp. 517–520.

Sohankar, A., Norberg, C., Davidson, L., 1997. Numerical simulation of unsteady low Reynolds number flow around rectangular cylinders at incidence. Journal of Wind Engineering and Industrial Aerodynamics 69–71, 189–201.

Sohankar, A., Norberg, C., Davidson, L., 1998. Low Reynolds number flow around a square cylinder at incidence: study of blockage, onset of vortex shedding and outlet boundary condition. International Journal for Numerical Methods in Fluids 26, 39–56.

Tamura, T., Ohta, I., Kuwahara, K., 1990. On the reliability of 2-D simulation for unsteady flows past a cylinder-type structure. Journal of Wind Engineering and Industrial Aerodynamics 35, 275–298.

Thames, F.C., Thompson, J.F., Mastin, C.W., Walker, R.L., 1977. Numerical solutions for viscous and potential flow about arbitrary two-dimensional bodies using body-fitted coordinate systems. Journal of Computational Physics 24, 245–273.

Torii, S., Yang, W.J., Umeda, S., 2000. Evolution of vortices behind single diamond-shaped cylinders in a free stream flow. Proceedings of the 2000 ASME/IMECE Conference, Orlando.

Zheng, W., Dalton, C., 1999. Numerical prediction of force on rectangular cylinders in oscillating viscous flow. Journal of Fluids and Structures 13, 225–249.